Penerbit Akademia Baru

Malaysian Journal on Composites Science and Manufacturing

Journal homepage:
https://www.akademiabaru.com/submit/index.php/mjcsm/
ISSN: 2716-6945

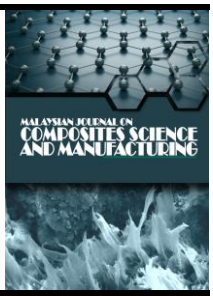

Numerical Investigation of Injection Pressure Effect on the Performance and Emission of a Diesel Engine Fuelled with Butanol-Diesel Blends

Open Access

Md Radwanul Kabir[1,*], Joy Ganguly[1], Md Sunney-ul-Alam[1], Sobahan Mia[1]

[1] Department of Mechanical Engineering, Khulna University of Engineering & Technology, Khulna- 9203 Bangladesh

ARTICLE INFO

Article history:
Received 28 October 2023
Received in revised form 27 February 2025
Accepted 18 March 2025
Available online 30 March 2025

Keywords:
Diesel engine, Injection pressure, Split Injection, Emission

ABSTRACT

Globally, fossil-based resources are becoming increasingly scarce as the demand for energy from power-producing systems rises. Diesel engines are a popular and efficient source of electricity, but different national and international organizations have imposed limits on diesel emissions. Reducing emissions and boosting performance are typical operations in diesel engines. ANSYS FORTE code was used to generate a thorough numerical configuration. Analyses were conducted on a single-cylinder, four-stroke, direct-injection diesel Cummins N-14 test engine setup running on a 40 percent butanol-diesel blend with injection pressure ranging from 400 bar to 1600 bar at constant speed conditions to determine its performance metrics (i.e. Thermal Efficiency & Specific Fuel Consumption), combustion attributes (i.e. In-cylinder Pressure, In-cylinder Temperature & Apparent Heat Release Rate), and emissions characteristics (i.e. CO emission, Nox emission & Soot emission). In general, as injection pressure was raised, thermal efficiency, CO emissions, and soot emissions all improved, while in-cylinder temperature, in-cylinder pressure & NOx emissions rose progressively. For instance, for 1400 bar fuel injection pressure, maximum in-cylinder pressure and in-cylinder temperature were found, around 18.6 bar and 1650 K, respectively, whereas injection started at a 22-degree crank angle before top dead center (bTDC). The optimal injection pressure for internal combustion engines was determined by considering both emissions and performance. The results indicated that an injection pressure near 800 bar led to the following outcomes: an in-cylinder temperature of approximately 1520 K, an in-cylinder pressure of around 17.5 bar, a thermal efficiency of 32.50%, and a specific fuel consumption of approximately 292 g/KW-h. Additionally, implementing a 90%-10% split injection method with equal crank angle duration (CAD) resulted in an average reduction of 4-6% in NOx emissions.

** Corresponding author.*
E-mail address: shuvo.redwan3.14159@gmail.com (Md. Radwanul Kabir)
E-mail of co-authors: joyganguly97.sghs@gmail.com, sunneyday2017@gmail.com, smia@me.kuet.ac.bd

https://doi.org/10.37934/mjcsm.16.1.118

1. Introduction

The world's need for energy must be met in large part by internal combustion engines. Because of their great thermal efficiency and low fuel consumption, diesel engines, in particular, have been widely employed in a variety of applications. Traditional diesel fuel use has released hazardous compounds into the environment, posing risks to human health and air quality. In recent years, declining crude oil supplies and rising prices have placed increasingly sensitive pressures on the trade balances of non-oil-producing countries while also posing a threat to the survival of developing and industrialized countries. Thus, considerable attention has been paid to the development of alternative fuel sources in various countries, with particular emphasis on bio-fuels that possess the added advantage of being renewable fuels that can be replenished through the growth of plants or production of livestock, showing an ad hoc advantage in reducing the emitted carbon dioxide. Butanol, a bio-alcohol, has recently gained attention as a potential replacement fuel for diesel vehicles. Butanol is preferable to ethanol for diesel engines due to its higher energy density and reduced volatility.[1] Fuel injection pressure may need to be adjusted when using a diesel-butanol blend, which may affect engine output and pollution levels. According to Krishna *et al*., [2] higher fuel injection pressure is preferable for smaller droplet sizes and leads to improved combustion. The best fuel injection pressure was found to be 210 bar, while diesel fuel was utilized in the injection pressure range of 180 bar to 240 bar. In this injection pressure, the emission is comparatively better. By increasing the injection pressure, NOx emissions are enhanced. Because of the high cylinder temperature, heptane fuel emits more NOx. Kannan *et al.* [3] carried out an experimental investigation on a light-duty direct injection diesel engine at 150, 200, and 250 bar injection. Performance and emission characteristics were graphed, and it was concluded that they were better at 200 bar fuel injection pressure for the light-duty engine.

Anuradha *et al*. [4] demonstrated a numerical analysis conducted on a light-duty direct injection diesel engine at 150 bar, 200 bar, and 250 bar injection pressures to investigate the influence on performance and emissions. The cylinder pressure increased by roughly 6 bar when the injection pressure was increased from 150 bar to 250 bar. When injection pressures were increased from 150 to 250 bars, the cylinder temperature rose by 16.9%. The generation of NOx increased by 41.5 percent. Keshav *et al.* [5] investigated the characteristics of high-pressure spray and exhaust emissions in a single-cylinder diesel engine using a common rail-type diesel fuel injector under various injector operation circumstances. An intensifier is used in the injection system to create pressure of up to 160 MPa. Abdullah *et al.* [7] adjusted the injection pressure from 300 to 800 bar using two different durations of main injection (dMI). A short dMI of 5 crank angle duration (CAD) before the main injection was studied, as was a long dMI 40 CAD before the main injection (main injection at 2.5 CAD after top dead Centre (aTDC) for 1500 rpm and 0.7 CAD aTDC for 2250 rpm). To investigate the effect at low load, engine speeds of 1500 rpm and 2250 rpm with loads of 35.1 Nm were chosen. When compared to water, the heat transfer coefficient is 25% higher. Aalam *et al*. [8] observed that employing an electronically controlled injection system and increasing the injector pressure from 220 bar to 1000 bar significantly improved performance and emissions due to better spray formation. Brake thermal efficiency rises from 23.8 to 29.2 percent, hydrocarbon emissions fall from 90 to 65ppm, and NOx emissions rise when injection pressure rises due to faster combustion and higher temperatures reached in the cycle. The amount of smoke emitted has been lowered from 64 to 46 HSU (Hartridge Smoke Unit).

In sharp contrast to the advanced models available for the study of diesel engines utilizing conventional diesel fuel [9-12], there is a scarcity of theoretical models addressing the mechanics of combustion-generated pollutants with liquid biofuels. Even though many experimental studies on

biofuel blends are accessible, the most effective fuel injection pressure is still under investigation [13, 14]. The experimental work is more expensive for engine studies. Therefore, simulation work is an efficient technique for determining the most effective operating state for an engine without changing any physical changes to the engine [15-18]. ANSYS Forte code is used in this study to find out the effect of fuel injection pressure ranging from 400 bar to 1600 bar more precisely performance metrics (i.e. Thermal Efficiency & Specific Fuel Consumption), combustion attributes (i.e. In-cylinder Pressure, In-cylinder Temperature & Apparent Heat Release Rate), and emissions characteristics (i.e. CO emission, NOx emission & Soot emission). Using the study result, the optimal fuel injection pressure range is determined. Most importantly, 90%-10% split injection method with an equal crank angle duration (CAD) of 10 degrees was introduced and studied in different injection pressure conditions ranging from 400 bar to 1400 bar. The emission characteristics of split fuel injection of variable injection pressure were analyzed.

2. Methodology

2.1 Numerical Model

Computational Fluid Dynamics (CFD) is a numerical analysis approach that analyzes the interaction of fluids with defined surfaces to solve fluid flow problems. Before being generally adopted, CFD simulation software was validated using an experimental apparatus and its association with experimental data. The simulation program ANSYS Forte provides freedom in building the computational mesh for describing system geometry. It has several mesh generation options, such as importing mesh definitions from other files and employing automatic or guided sector mesh generators for engine simulations. In ANSYS Forte, the workflow tree provides a step-by-step navigation mechanism for configuring and executing simulations and easy access to various panels for input and simulation parameters. The workflow tree's nodes can be configured at any moment, and additional elements can be added based on configuration choices. The simulation covers only the closed portion of the engine cycle, from intake valve closure (IVC) at 120° before the top dead center(bTDC) to the exhaust valve opening (EVO) at 125° after the top dead center (aTDC).

Table 1
Cummins N-14 Engine Specification[1]

Feature	Value
Speed (RPM)	1200
IMEP (bar)	4
Intake Temp (°C)	111
BDC Temp (°C)	106
Intake Pressure (kPa)	233
TDC Motored Temp. (K)	905
TDC Motored Density (kg/m^3)	24
Peak Adiabatic Flame Temp [K]	2760
SOI (°aTDC)	-7
Injection Quantity (mg)	61
DOI (CAD)	10
O_2 Conc. (Vol %)	21

The simulation was carried out using a four-stroke Diesel Cummins N-14 direct injection single-cylinder test engine (Table 1). The Bowl Profile, the curved shape on the piston surface, can be

defined using one of six alternative mesh topology examples provided by ANSYS Forte. Bore, stroke, squish, crevice width, and crevice height are just some of the engine characteristics that may be adjusted in the workflow tree of the Forte Sector Mesh Generator (Figures 1 and 2). It was configured to compress at an 18:1 ratio. The key parameters used in this case were 13.97 cm for the bore diameter, 15.24 cm for the stroke, 0.56 cm for the squish, 0.167 cm for the crevice width, and 3.72621 cm for the crevice height. There was a 45-degree angle in the section. Mesh creation was chosen for the third topology. The mesh topology's control point positions and the distance between them in cells can both be specified as needed. Table 2 shows the scope and simulation solver models, and Figure 3 lists the steps of ANSYS Forte Simulation.

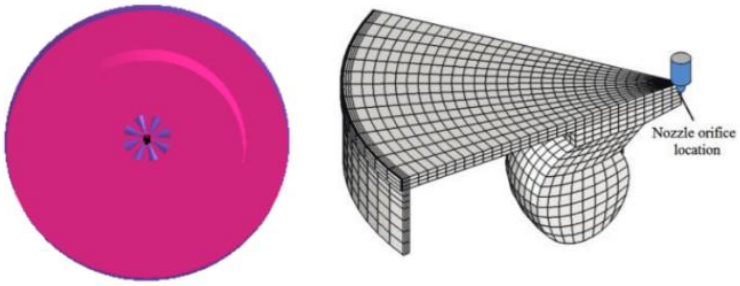

Fig. 1. Sector mesh dividing the nozzles

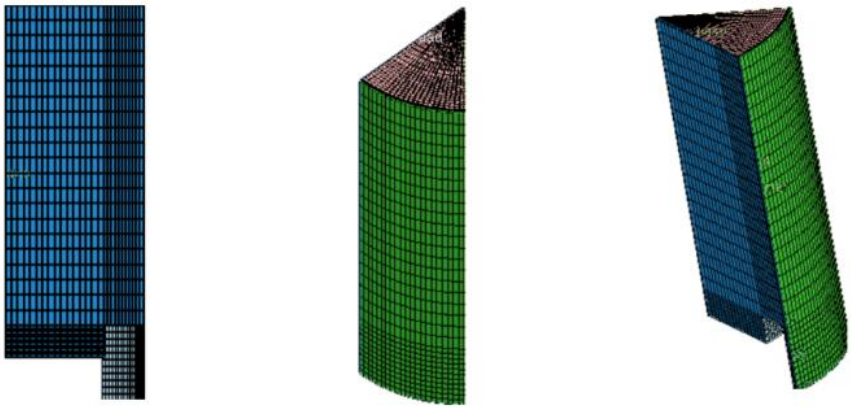

Fig. 2. Generated sector mesh

Table 2
Simulation solver model

Scope	Solver Model
Chemical Kinetics	Equation of State: Ideal gas Chemkin Chemistry Set: Diesel-Butanol chemistry file
Flame Speed Model	Laminar Flame Speed: Power law
Transport	Turbulence: RNG k-ε
Spray Model	Droplet Model: Radius of Influence Solid Cone Breakup Model: Gas Jet Model, RT Model, KH Model
Soot Model	Two-step model

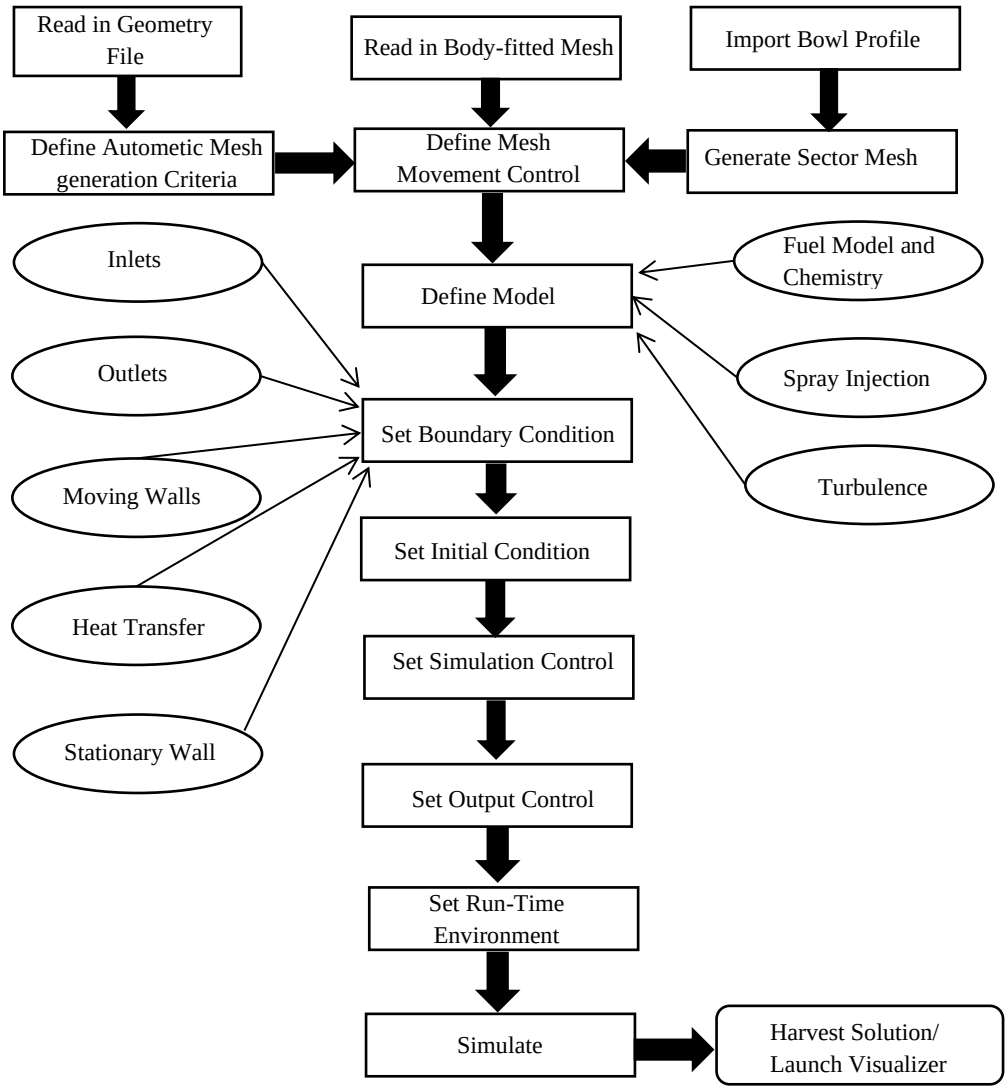

Fig. 3. Steps of ANSYS Forte Simulation

2.2 Governing Equations

The fuel-air combination and the byproducts of combustion are the working fluids, respectively, before and after combustion. The Navier-Stokes equations govern the fundamental fluid dynamics in ANSYS Forte's description of turbulent reactive flow. For compressible, gas-phase flows, the turbulent character of the flow was demonstrated by establishing model transport equations that include mass, momentum, and energy conservation laws. Exchange functions were utilized to account for the interaction between the gas phase and liquid droplets when liquid sprays were introduced into the flow. In addition to these models, the governing equations were derived using the ideal gas law for the gas-phase equation of state and Fick's law for mass transport.

2.2.1 Equation for the Conservation of Species

Convection, molecular diffusion, turbulent transport, interactions with fuel sprays, and combustion all contribute to the dynamic nature of the gas-phase working fluids of a combustion engine, whereas those gas-phase working fluids were formed from a combination of discrete gas

components, or species or a mixture of vaporized fuel and air particles. The conservation equation for the mass of species k is:

$$\frac{\partial \bar{\rho}_k}{\partial t} + \nabla(\bar{\rho}_k \tilde{u}) = \nabla[\bar{\rho}_k D \bar{y}_k] + \nabla + \varphi \qquad (Here, k = 1,2,3, \dots K)\ [19] \tag{1}$$

Here, ρ is the density, u is the velocity vector of the flow, K is the total number of species, and k denotes the index of all those species. The effects of ensemble averaging or convection term filtering are taken into consideration by the φ term, that is $\varphi = \bar{\rho}_k \tilde{u} - \overline{\bar{\rho}_k u}$.

2.2.2 A Continuity Theorem Used for Fluids

For a fluid in its whole, the gas phase continuity equation [19] is as follows:

$$\frac{\partial \bar{\rho}}{\partial t} + \nabla(\bar{\rho}\tilde{u}) = \overline{\rho^s} \tag{2}$$

Here, $\frac{\partial \bar{\rho}}{\partial t}$ represents the time rate of change of density within a control volume, $\nabla(\bar{\rho}\tilde{u})$ is the divergence of the product of density (ρ) and velocity (u), which basically represents the spatial rate of flow out of the control volume, and $\overline{\rho^s}$ is a source term due to chemical reactions and spray evaporation.

2.2.3 Equation for the Conservation of Momentum

The effects of liquid sprays and body force are included in the momentum equation, along with those of convection, pressure force, viscous stress, and turbulent transport [19] :

$$\frac{\partial \bar{\rho}\tilde{u}}{\partial t} + \nabla(\bar{\rho}\tilde{u}\tilde{u}) = -\nabla\bar{p} + \nabla\bar{\sigma} - \frac{2}{3}\bar{\rho}\tilde{k}I + \bar{F}^S + \bar{\rho}\bar{g} \tag{3}$$

In Eq. 3, p represents the pressure, $\bar{F}^S$ represents the momentum gain per unit volume caused by the spray, $\bar{g}$ represents the body force, $\bar{\sigma}$ represents the viscous shear stress, and I is the identity tensor. Turbulence models were needed to provide closure in both the RANS and LES approaches.

2.2.4 Energy Conservation Equation

Based on the First Law of Thermodynamics, the alteration in internal energy must be balanced by pressure work and heat transfer. The effects of convection, turbulent transport, turbulent dissipation, sprays, chemical reactions, and enthalpy diffusion in a multi-component flow should also be considered while solving flow problems associated with internal combustion engines. The internal energy transport equation [19] is:

$$\frac{\partial \bar{\rho}\tilde{I}}{\partial t} + \nabla(\bar{\rho}\,\widetilde{u}\tilde{I}) = -\bar{\rho}\nabla\widetilde{u} - \bar{p}\nabla\tilde{u} - \nabla\tilde{J} - \nabla H + \bar{\rho}\tilde{\varepsilon} + \bar{Q}^C + \bar{Q}^S \tag{4}$$

$\frac{\partial \bar{\rho}\tilde{I}}{\partial t}$ represents the time rate of change of mean internal energy (I) per unit volume, where ρ is the density of the fluid, $\nabla(\bar{\rho}\,\widetilde{u}\tilde{I})$ is the divergence of the product of mean density (ρ), mean velocity (u), and mean internal energy (I), representing the convective transport of energy, $\bar{\rho}\nabla\widetilde{u}$

represents the work done by the Reynolds stress (turbulent stress) in the flow, $\bar{p}\nabla\tilde{u}$ represents the work done by the pressure forces in the flow, $\nabla\tilde{J}$ represents the diffusion of heat due to temperature gradients, where J is the heat flux vector, ∇H represents the enthalpy gradient in the flow, $\bar{\rho}\tilde{\varepsilon}$ represents the dissipation rate of turbulent kinetic energy into internal energy due to viscosity, $\bar{Q}^C$ could represent a source term for heat addition or removal due to chemical reactions and $\bar{Q}^S$ could represent a source term for heat addition or removal due to external sources (like heating or cooling).

2.2.5 Method Based on Reynolds Averaged Navier Stokes (RANS)

The RANS approach aims to simulate the ensemble-averaged flow field. The most common method is using gradient-diffusion assumptions to model the turbulent transport processes. The Reynolds stress has deviatoric components that are directly proportional to the mean deviatoric strain rate in the momentum equation. The Reynolds stress tensor [19] can be thought of as:

$$\Gamma = -\bar{\rho}\vartheta_T\left[\nabla\tilde{u}(\nabla\tilde{u})^T - \frac{2}{3}(\nabla\tilde{u})I\right] + \frac{2}{3}\bar{\rho}\tilde{k}I \tag{5}$$

If the dissipation rate is ε and the turbulent kinematic viscosity is ϑ_T [19], then.

$$\vartheta_T = C_\mu\frac{\tilde{k}^2}{\tilde{\varepsilon}} \tag{6}$$

Here C_μ is a model constant that varies in different turbulence model formulations.

The kinetic energy of the turbulent flow $\tilde{k}$ [19], which is defined as:

$$\tilde{k} = \frac{1}{2\rho}trace(\Gamma) = \frac{1}{2}\overline{u^{"}u^{"}} \tag{7}$$

Here, $u^{"}$ represents the fluctuating velocity components due to turbulence, and the overbar indicates an average. The product of the fluctuating velocities squared, averaged, and multiplied by 1/2 gives the turbulent kinetic energy.

In ANSYS Forte, both the standard and the advanced (based on Re-Normalized Group Theory) *k-ε* model formulations are available. These consider velocity dilatation in the ε- equation and spray-induced source terms for both k and ε equations.

The usual Favre-averaged formulae for k-ε [19] are as follows:

$$\frac{\partial\bar{\rho}\tilde{k}}{\partial t} + \nabla\left(\bar{\rho}\,\tilde{u}\tilde{k}\right) = -\frac{2}{3}\tilde{\rho}\tilde{k}\nabla\tilde{u} + (\tilde{\sigma} - \Gamma):\nabla\tilde{u} + \nabla.\left[\frac{\mu+\mu_T}{P_{r_k}} + \nabla\tilde{k}\right] - \overline{\rho\varepsilon} + \bar{W}^s \tag{8}$$

$$\frac{\partial\bar{\rho}\tilde{\varepsilon}}{\partial t} + \nabla(\bar{\rho}\,\tilde{u}\tilde{\varepsilon}) = -\left(\frac{2}{3}C_{\varepsilon_1} - C_{\varepsilon_2}\right)\tilde{\rho}\tilde{\varepsilon}:\nabla\tilde{u} + \nabla.\left[\frac{\mu+\mu_T}{P_{r_\varepsilon}} + \nabla\tilde{\varepsilon}\right] + \frac{\tilde{\varepsilon}}{k}\left(C_{\varepsilon_1}(\sigma - \Gamma):\nabla\tilde{u} - C_{\varepsilon_2}\tilde{\rho}\tilde{\varepsilon} + C_s\bar{W}^s\right) \tag{9}$$

In these equations, $P_{r_k}, P_{r_\varepsilon}$, C_s, C_{ε_1} ,C_{ε_2} are model constants. The source terms involving $\bar{W}^s$ is calculated based on the droplet probability distribution function.

2.2.6 Synthesis of Chemical Kinetics

The chemical reactions that occur in combustion simulations can be characterized by chemical kinetic mechanisms, which define the reaction routes and the related reaction rates leading to the change in species concentrations. Reversible(or irreversible) processes involving *k* chemical species can be expressed by this general form in precise chemical kinetic mechanisms [19]:

$$\sum_{k=1}^{k} v'\ ki^{\chi}k \Leftrightarrow \sum_{k=1}^{k} v''\ ki^{\chi}k\ (i = 1, \dots, I). \tag{10}$$

The rate at which the k^{th} species is formed in the *i*-th reaction [19] can be expressed as:

$$\dot{\omega}_{ki} = (v''_{ki} - v'_{ki})q_i(k = 1, \dots, K) \tag{11}$$

where q_i is the rate of progress of reaction i.

In the species continuity equation, the chemical source term $\dot{\rho}_k^c$ is obtained by adding up $\dot{\omega}_{ki}$ to all the reactions [19]:

$$\dot{\rho}_k^c = W_k \sum_{i=1}^{I} \dot{\omega}_{ki} \tag{12}$$

The corresponding term in the energy equation for the release of chemical heat is [8, 19]:

$$\dot{Q}_c = -\sum_{i=1}^{I} Q_i\, q_i\ = \sum_{i=1}^{I}\sum_{k=1}^{K}(v''_{ki} - v'_{ki})\left(\Delta h_f^0\right)_k q_i\,, \tag{13}$$

Where Q_i is the heat of reaction *i* at absolute zero [19]:

$$Q_i\ = \sum_{k=1}^{K}(v''_{ki} - v'_{ki})\left(\Delta h_f^0\right)_k, \tag{14}$$

And $\left(\Delta \mathrm{h}_\mathrm{f}^0\right)_\mathrm{k}$, represents the heat required to create species k at absolute zero.

2.3 Fuel Injection Pressure and Fuel Specification

A fuel injector was used for the simulation, whereas eight equally spaced nozzles were set. Seven different injection pressures (400, 600, 800, 1000, 1200, 1400 and 1600 bar) were tested with a varying nozzle diameter while the engine rotated at 1200 rpm. Also, a butanol-diesel blend of 40% (40% butanol and 60% diesel) fuel was used to create the fuel mixture. The fuel specifications are shown in Table 3.

2.3.1 Split Injection Setup

There were two split injection pulses with a 10-degree crank angle interval. The duration of both injections was 10° crank angle, while the fuel's entire mass flow rate was divided into two portions of 90% and 10%, respectively. Fuel injection pressure was set similarly as before.

Table 3
Fuel Specifications

Property	Diesel	Butanol
Mass per volume (in kg/L)	0.82–0.86	0.810
Kinematic Viscosity (mm^2/s) at 40 °C	2.7	2.22
Calorific values (MJ/kg)	42.8	33.1
Maximum temperature at which water can be boiled (°C)	210–235	118
Latent heat of vaporization (kJ/kg)	270	582
Auto-ignition temperature (°C)	≈300	385
Surface tension (mN/m)	23.8	24.2

2.4 Initial Condition

The simulation only includes the closed fluid portion of the engine cycle, from 120° before the top dead center (bTDC) to 125° after the top dead center (aTDC). As a result, initial pressure, temperature, species composition (such as air or a fuel-air combination), turbulence kinetic-energy intensity (TKEI), and turbulence length scale (TLS) were all part of each computational region's initial circumstances. Initial conditions were uniform and obtained from an intake stroke simulation for engine sector simulations. In some models, the initial momentum brought on by swirl flow was also considered. O_2 and N_2 were presented in the composition at mole fractions of 0.126 and 0.874, respectively. The pressure was 2.215 bar, and the initial temperature was set at 362.0 K. With a TKEI of 10,000 cm^2/sec^2 and a Turbulent Length Scale of 1.0 cm, the turbulence remained continuous. A Bessel function profile was used to represent the swirl component of the flow, and the initial swirl ratio was set to 0.5.

2.5 Boundary Condition

As the fluid portion of the engine cycle was solely included in the simulation, boundary condition choices provided by ANSYS Forte include inflow, outflow, stiff walls of the engine cylinder and piston, periodic, and symmetry. In cylinder simulations, using walls with constant temperatures and turbulent rules for velocity conditions is common. For N-fold periodicity, periodic boundaries were employed, as in sector mesh simulations. The Law of the Wall accurately describes the effects of wall boundary layers. It is possible to specify piston motion and heat transmission to wall borders. Specific values assigned in the study for piston boundary condition include piston temperature (500.0 K), motion type (slider crank), stroke length (152.4 mm), bore diameter (139.7 mm), connecting rod length (304.8 mm), piston offset (0.0), head temperature (470.0 K), liner temperature (420.0 K) and heat transfer model (Han Reitz Model). For periodicity, the assigned value was sector angle (45°).

2.6 Model Validation

In this study, ANSYS Forte 2022 R1 software was utilized to validate a simulation model against experimental data from a Cummins N-14 test engine. The engine was fueled with 100% n-heptane as a substitute for diesel fuel. Model validation involved comparing experimental measurements with numerical simulation results. Key validation criteria included peak in-cylinder pressure, overall pressure profile shape, and heat release rate. Figure 4 shows a comparison between the simulated

and experimental heat release rate curves, while Figure 5 shows the simulated and experimental pressure profiles.

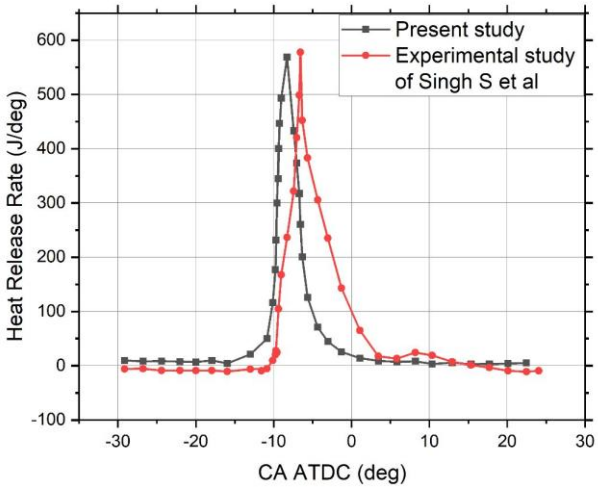

Fig. 4. The Rate of Heat Release for 100 percent diesel was compared to experimental data from Singh *et al*.[1]

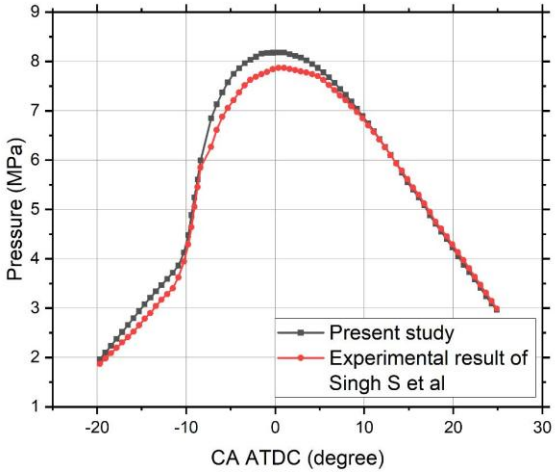

Fig. 5. Comparison of Pressure for Diesel 100% with experimental of Singh *et al.*[1]

The peak magnitude and duration of the heat release were consistent between the simulated and experimental data. From 10 degrees before TDC to 15 degrees after TDC, the pressure distribution trends were identical in both cases, despite errors in in-cylinder pressure and heat release rate. The values of the peak in-cylinder pressure were predicted with less than 12% deviation from the experimental profile, while those of the heat release rate were predicted with a maximum error of approximately 5%. Due to the lack of data, the average assumptions were made, impacting the simulation's capacity to be perfectly validated. Despite variations in pressure profiles, both cases show a constant upward trend in cylinder pressure.

3. Results

3.1 Effect of Injection Pressure on In-cylinder Characteristics

The cylinder pressure, apparent heat release rate (AHRR), and in-cylinder temperature of a combustion engine all respond differently to changes in injection pressure. At low injection pressures, both cylinder pressure and AHRR decreased. However, due to improved fuel-air mixing and a more thorough combustion process, cylinder pressure and AHRR increased as injection pressure rose. These changes resulted in higher efficiency and lower emissions. However, at very high injection pressures, such as 1600 bar, cylinder pressure could plateau or decrease due to overly rapid combustion, leading to pressure waves that might harm the engine. Therefore, reducing the injection pressure is crucial for ensuring a safe and reliable engine operation under such conditions.

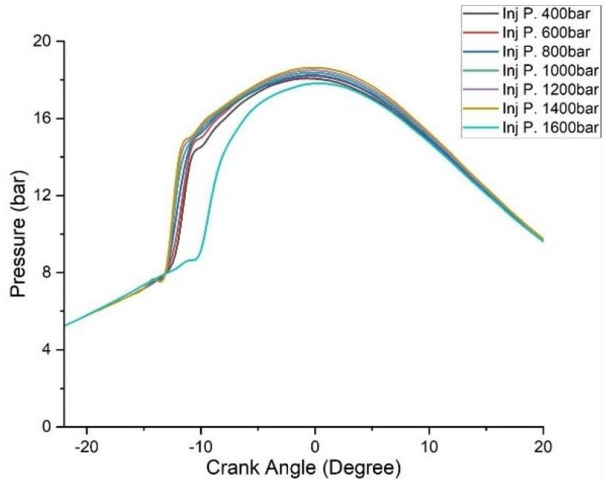

Fig. 6. Pressure variations with in-cylinder Crank Angle for different injection pressure

Figure 6 illustrates the relationship between in-cylinder pressure and crank angle in a diesel engine, with different lines representing various fuel injection pressures. As the fuel injection pressure increased, the peak in-cylinder pressure also increased. This indicated that higher injection pressures could enhance combustion efficiency. For instance, the maximum in-cylinder pressure for a 1400 bar fuel injection pressure was around 18.6 bar. The peak pressure occurred at an earlier crank angle with higher injection pressures. This suggested that combustion started sooner when the fuel was injected at higher pressures. This observation was verified by noting the drastic increase in in-cylinder pressure at around -14° crank angle for the injection pressure of 1400 bar, whereas injection started at a 22-degree crank angle before the top dead center (bTDC).

Figure 7 shows a graph that plots in-cylinder temperature against crank angle for different fuel injection pressures in a diesel engine. As the crank angle approached the top dead center (0 degrees), the in-cylinder temperature rose, peaking shortly after. Higher fuel injection pressures resulted in higher peak temperatures. For example, at 400 bar, the peak temperature was just above 1400 K. At 1400 bar, the peak temperature reached nearly 1650 K. The numerical data indicated that for every 200 bar increase in injection pressure, there was a significant increase in peak temperature, validating the trend that higher pressures led to higher in-cylinder temperatures.

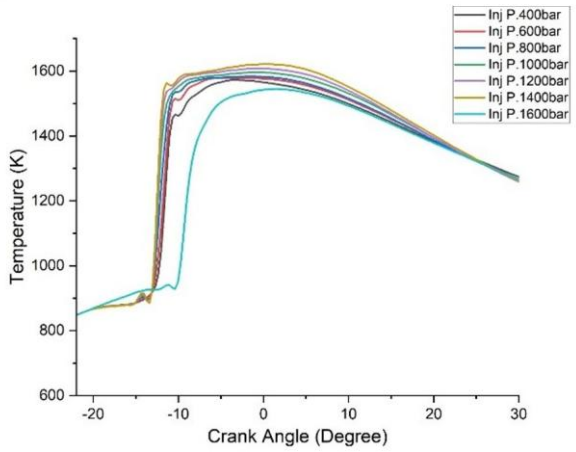

Fig. 7. Temperature variations with in-cylinder Crank Angle for different injection pressure

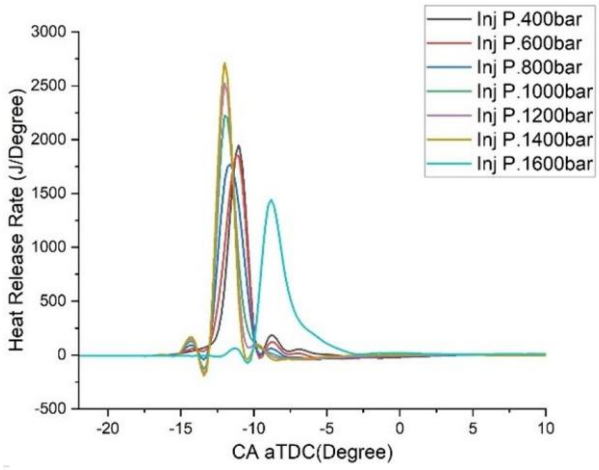

Fig. 8. Apparent Heat Release Rate variations with in-cylinder Crank Angle for different injection pressure

Figure 8 shows the relationship between in-cylinder heat release rate and crank angle for different fuel injection pressures in a diesel engine and illustrates how varying pressures impact the combustion process. As the fuel injection pressure increased, the peak heat release rate also increased. This suggested that higher pressures improved combustion efficiency, leading to a more intense and quicker burn. The trend is clear from the graph: higher injection pressures resulted in higher and earlier peaks in heat release rate, which benefited engine efficiency and power output.

Regarding in-cylinder temperature, finer fuel droplets, better atomization, and better mixing of the air-fuel combination all contributed to higher temperatures as injection pressure increased. These elements improved combustion effectiveness. However, raising injection pressure even more after a certain level (for instance, 1400 bar) could lower in-cylinder temperatures. This was because atomized fuel required less time to mix, and some fuels, such as butanol, vaporized at higher temperatures than diesel fuel, which could have a cooling impact. As a result, temperatures might drop close to the fuel spray. In conclusion, although the link between in-cylinder temperature and injection pressure tended to increase, it could be altered by factors such as engine design, fuel characteristics, and operating conditions, making it a complex phenomenon.

3.2 Effect of Injection Pressure on Emission Characteristics

Injector pressure affected diesel engine combustion efficiency and pollution output. Incomplete combustion occurred at low injection pressures, leading to higher particulate matter emissions and unburned hydrocarbons. Increasing the pressure improved combustion, but it also raised NOx emissions. If the pressure was too high, the fuel spray became too atomized, resulting in increased NOx emissions. While soot emissions were engine- and operation-specific, higher injection pressures often reduced soot emissions. Fuel droplets were more easily broken apart at higher injection pressures, leading to better mixing and less CO production—two factors crucial to efficient combustion.

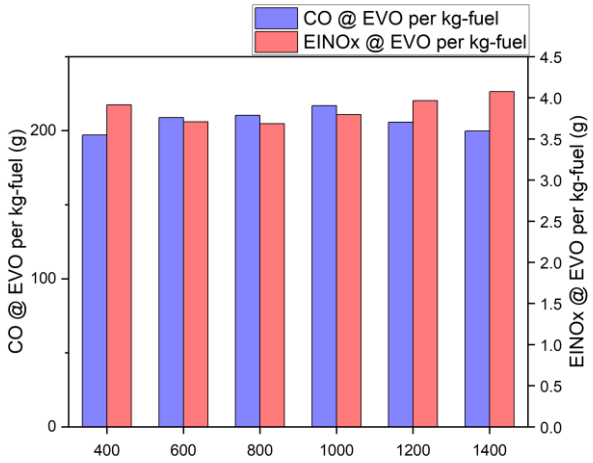

Fig. 9. Comparison of Nitrogen Oxides (NOx) and Carbon Monoxide (CO) emission at Exhaust Valve Opening (EVO)

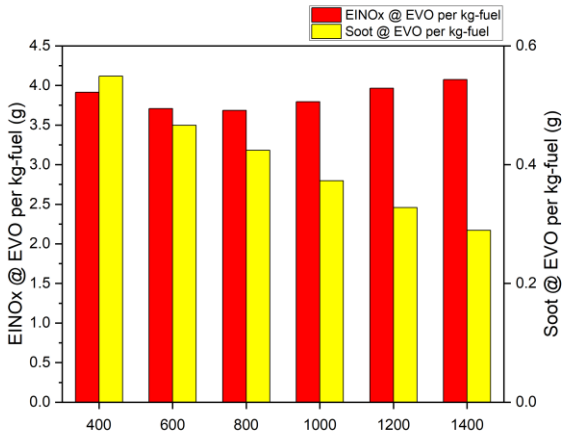

Fig. 10. Comparison of Nitrogen Oxides (NOx) and Soot emission at Exhaust Valve Opening (EVO)

Figure 9 shows data demonstrating a connection between injection pressure and carbon monoxide and nitrogen oxide emissions. Variations in CO and NOx emissions were observed at injection pressures ranging from 400 to 1400 bar. CO emission, on the other hand, showed a general downward trend, with the lowest value recorded at 800 bar of injection pressure. However, NOx emission exhibited a more erratic pattern, increasing somewhat between 400 and 600 bar, then decreasing until 1000 bar, and then increasing again between 1200 and 1400 bar. This occurred

because specific fuel consumption was greater at lower fuel injection pressure, resulting in a lower air-fuel ratio in the combustion chamber. Consequently, irregular combustion took place, and NOx generation was greater when injection pressure was low. On the other hand, NOx generation was also higher at greater injection pressure because higher injection pressure led to better combustion and higher in-cylinder temperature, which was a dominant factor for high NOx emission.

Figure 10 depicts the results of an analysis of the dataset representing the relation between injection pressure and NOx and soot emissions. Soot emissions decreased as the injection pressure rose from 400 to 1400 bar. When the injection pressure was raised, the emission index for soot decreased. For instance, soot emission reached its lowest point at an injection pressure of 1400 bar.

In the end, the injection pressure played a significant role in diesel engine emissions and combustion efficiency. Complete combustion was promoted by the optimal injection pressure, reducing emissions of soot, particles, and unburned hydrocarbons. However, there was a fine line to walk when determining the optimal injection pressure, as doing so could lead to an increase in NOx emissions and complicated consequences for soot emissions. Combustion efficiency and reduced CO emissions depended on the atomization and mixing of fuel.

3.3 Effect of Injection Pressure on Thermal Efficiency and Specific Fuel Consumption

More energy was converted and burned from fuel when the injection pressure was increased, as observed in Figure 11. However, progress slowed down significantly at high injection pressures. Increasing injection pressure led to a higher specific fuel consumption, indicating more efficient combustion and less wasted fuel in the exhaust. Overall thermal efficiency and fuel consumption had adverse effects with increasing injection pressure, yet there was an optimal situation for producing maximum effective output.

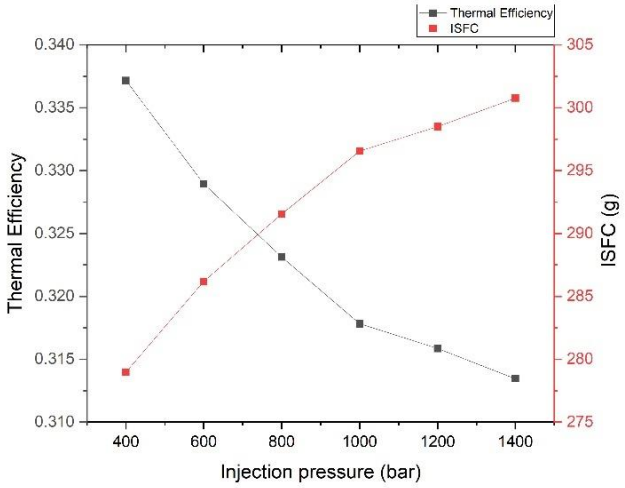

Fig. 11. Comparison of Thermal Efficiency with Indicated Specific Fuel Consumption (ISFC)

As a result, the optimum injection pressure for a 40% butanol-diesel blend was 800 bar, considering the emission of NOx, CO, and soot. Additionally, thermal efficiency and fuel consumption positively influenced the decision on the optimal injection pressure.

3.4 Emission Effect of Split Injection on Variable Injection Pressure

Two split injection pulses with 10-degree crank angle intervals were used to achieve a split injection outcome. The duration of both injections was 10 degrees of crank angle, while the fuel's overall mass flow rate was divided into two portions of 90% and 10%, respectively. Figures 12 and 13 showed that split injection significantly reduced NOx emissions compared to non-split injection, with an average reduction of 4%. Thus, it was evident that split injection contributed to NOx reduction.

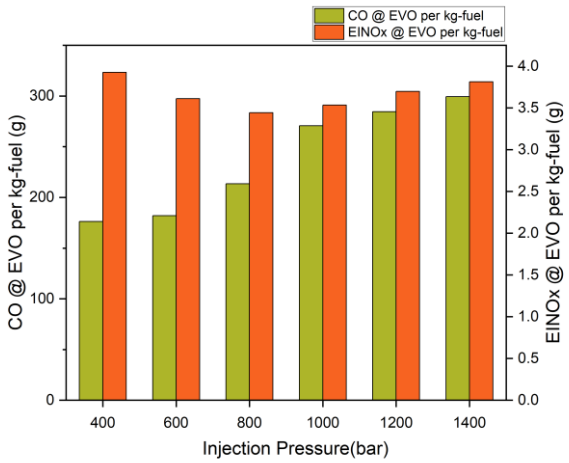

Fig. 12. Comparison of CO and NOx at Exhaust Valve Opening (EVO) in Condition of Specific Split Injection

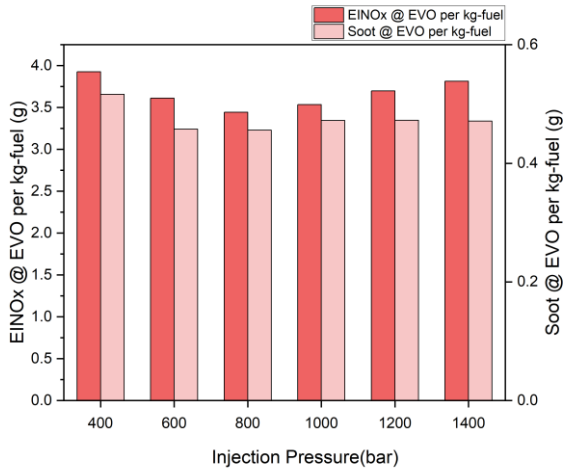

Fig. 13. Comparison of Soot and NOx at Exhaust Valve Opening (EVO) in Condition of Specific Split Injection

On the other hand, CO emission decreased significantly with the reduction of injection pressure, indicating more efficient combustion. Additionally, this suggested that using split injection reduced the need for excessive injection pressure. Soot emission improved, and after an injection pressure of 800 bar, soot emission remained nearly constant.

Analyzing the above dataset, an injection pressure of 700 bar might provide the optimum pressure considering the lowest emissions. Furthermore, it was evident that split injection enhanced emission characteristics more than single injection at slightly lower injection pressure.

4. Conclusions

Conducting engine research to advance the automotive sector and enable incremental engine improvement is essential. This particular study emphasizes Injection Pressure with performance metrics (i.e. Thermal Efficiency and Specific Fuel Consumption), combustion attributes (i.e. In-cylinder Pressure, In-cylinder Temperature & Apparent Heat Release Rate), and emissions characteristics (i.e. CO emission, NOx emission and Soot emission) to comprehend the impact of engines on the combustion process. Moreover, it investigates the emission impacts of Split Injection with Variable Injection Pressure.

The outcomes of this investigation can be summarized as follows:

i. Increasing the injection pressure causes the cylinder pressure and heat release rate to rise, suggesting that the combustion process intensifies and becomes more effective, increasing power output and performance. For instance, for 1400 bar fuel injection pressure, maximum in-cylinder pressure and in-cylinder temperature were found, around 18.6 bar and 1650 K, respectively.
ii. Increased injection pressure leads to higher NOx emissions and elevated cylinder temperatures. At an injection pressure of 1400 bar, NOx emissions reach 4 g per kg of fuel at the exhaust valve opening. Striking a balance that satisfies both performance and environmental criteria is crucial, even if it involves a trade-off between improved combustion efficiency and potentially higher emissions.
iii. The study revealed a positive outcome: minimal soot generation with higher injection pressure. Soot, a byproduct of incomplete combustion, contributes to particulate matter emissions and air pollution. The decrease in soot indicates cleaner and more complete combustion. Specifically, when shifting injection pressure from 600 to 800 bar, soot emissions decreased by nearly 6%.
iv. Another significant finding relates to combustion duration. Higher injection pressure leads to shorter combustion duration. This implies that fuel burns more rapidly and efficiently, enhancing engine responsiveness and reducing fuel consumption. Notably, at an injection pressure of 1400 bar, there was a drastic increase in in-cylinder pressure around -14° crank angle, while injection starts at a 22-degree crank angle before the top dead center (bTDC).
v. Split injection offers a solution to high injection pressure requirements. This resulted in a reduction of NOx emissions of 4-6% on average. Additionally, lowering injection pressure leads to reduced CO emissions—a clear sign of improved combustion efficiency when employing split injection.

This research underscores the critical role of optimizing injection pressure for engine performance. By comprehending the effects of higher injection pressure—such as increased cylinder pressure and temperature, NOx emissions, minimal soot production, and shortened combustion time—engineers can strike a delicate balance between performance, efficiency, and emission management in the design of modern engines.

Acknowledgment
The writer wishes to offer their deepest appreciation and acknowledgement to the Department of Mechanical Engineering, KUET, for all the help and support in properly conducting this simulation work.

References

[1] Singh, Satbir, Rolf D. Reitz and Mark P. B. Musculus, "Comparison of the Characteristic Time (CTC), Representative Interactive Flamelet (RIF), and Direct Integration With Detailed Chemistry Combustion Models Against Optical Diagnostic Data for Multi-Mode Combustion in a Heavy-Duty DI Diesel Engine," SAE Technical Papers, (2006): 61-82. https://doi.org/10.4271/2006-01-0055

[2] Maneesh Krishna, T., Biju Cherian Abraham, Arjun Baby and Jibin Alex, "Numerical Analysis of Effect of Injection Pressures on Emissions of Direct Injection Diesel Engine Fuelled with Diesel and Heptane," International Research Journal of Engineering and Technology 5, no. 4 (2018): 3970-3977. https://www.irjet.net/archives/V5/i4/IRJET-V5I4887.pdf

[3] Kannan, K. and M. Udayakumar, "Experimental Study of the Effect of Fuel Injection Pressure on Diesel Engine Performance and Emission," ARPN Journal of Engineering and Applied Sciences 5, no. 5 (2010): 42–45.

[4] C. Anuradha, T. Anand Kumar, M. Lakshmi Kantha Reddy and Dr. G. Prasanthi, "Effect of Injection Pressures on Emissions of Direct Injection Diesel Engine by Using CFD Simulation," IOSR Journal of Mechanical and Civil Engineering 13, no. 05 (2016): 15–19. https://doi.org/10.9790/1684-1305051519

[5] C. Anuradha, T. Anand Kumar, Dr. M. Lakshmi Kantha Reddy and Dr. G. Prasanthi, "Effect of Injection Pressures on Emissions of Direct Injection Diesel Engine By Using CFD Simulation," IOSR Journal of Mechanical and Civil Engineering 13, no. 5 (2016): 15–19. https://www.iosrjournals.org/iosr-jmce/papers/vol13-issue5/Version-5/B1305051519.pdf

[6] Varde, Keshav S., and Takashi Watanabe, "Characteristics of High-Pressure Spray and Exhaust Emissions in a Single-Cylinder Di Diesel Engine," SAE Technical Paper (2000): 1-7. https://www.sae.org/publications/technical-papers/content/2000-05-0333/

[7] Nik Rosli Abdullah, Rizalman Mamat, Paul Rounce, M. L. Wyszynski, Athanasios Tsolakis, H. M. Xu and Guohong Tian, "The Effect of Injection Pressure and Strategy in a Jaguar V6 Diesel Engine," Journal of KONES Internal Combustion Engine 16, no. 2 (2009): 9–22.

[8] C. Syed Aalam and C. G. Saravanan, "Effects of Fuel Injection Pressure on CRDI Diesel Engine Performance and Emissions Using CCD," International Research Journal of Engineering and Technology 2, no. 5 (2015): 1411–1416. https://www.irjet.net/archives/V2/i5/IRJET-V2I5228.pdf

[9] Carlucci, A.P., F.F. Chiara and D. Laforgia, "Analysis of the Relation Between Injection Parameter Variation and Block Vibration of an Internal Combustion Diesel Engine," Journal of Sound and Vibration 295, no. 1–2 (2006): 141–64. https://doi.org/10.1016/j.jsv.2005.12.054

[10] Mulemane, Aditya, Joong-Sub Han, Pai-Hsiu Lu, Suck-Ju Yoon and Ming-Chia Lai, "Modeling Dynamic Behavior of Diesel Fuel Injection Systems," SAE Technical Papers on CD-ROM/SAE Technical Paper Series, March 8 (2004). https://doi.org/10.4271/2004-01-0536

[11] Payri, F, A Broatch, B Tormos and V Marant, "New Methodology for In-cylinder Pressure Analysis in Direct Injection Diesel Engines—application to Combustion Noise," Measurement Science & Technology 16, no. 2 (2005): 540–547. https://doi.org/10.1088/0957-0233/16/2/029

[12] G, Prabhakara Rao, V.R.K. Raju, and S. Srinivasa Rao, "Effect of Fuel Injection Pressure and Spray Cone Angle in DI Diesel Engine Using CONVERGETM CFD Code," Procedia Engineering 127, (2015): 295–300. https://doi.org/10.1016/j.proeng.2015.11.372

[13] Xiaofeng Wang, Xinhua Liang, Jiaomin Li and Qingbo Li, "Catalytic Hydrogenolysis of Biomass-Derived 5-Hydroxymethylfurfural to Biofuel 2, 5-Dimethylfuran," Applied Catalysis A: General, vol. 576, (2019): 85 - 95. https://doi.org/10.1016/j.apcata.2019.03.005

[14] Agarwal, Avinash Kumar, Dhananjay Kumar Srivastava, Atul Dhar, Rakesh Kumar Maurya, Pravesh Chandra Shukla and Akhilendra Pratap Singh, "Effect of Fuel Injection Timing and Pressure on Combustion, Emissions and Performance Characteristics of a Single Cylinder Diesel Engine," Fuel 111 (2013): 374–83. https://doi.org/10.1016/j.fuel.2013.03.016

[15] Rizvi, Ikhtedar Husain, and Rajesh Gupta, "Numerical Investigation of Injection Parameters and Piston Bowl Geometries on Emission and Thermal Performance of DI Diesel Engine," SN Applied Sciences 3, no. 6 (May 12, 2021). https://doi.org/10.1007/s42452-021-04633-1

[16] De Syniawa, Larisa Leon, Reddy Babu Siddareddy, Sascha Prehn, Vivien Guenther, Tim Franken, Bert Buchholz and Fabian Mauß, "Simulation of CNG Engine in Agriculture Vehicles. Part 2: Coupled Engine and Exhaust Gas Aftertreatment Simulations Using a Detailed TWC Model," SAE Technical Papers on CD-ROM/SAE Technical Paper Series, August 28, 2023. https://doi.org/10.4271/2023-24-0112

[17] Yu, Weigang, Zhiqing Zhang and Bo Liu, "Investigation on the Performance Enhancement and Emission Reduction of a Biodiesel Fueled Diesel Engine Based on an Improved Entire Diesel Engine Simulation Model," Processes 9, no. 1 (January 6, 2021): 104. https://doi.org/10.3390/pr9010104
[18] Ogata, Kenichiro, Hiromitsu Matsuda, Haruna Kawai, and Keiji Shiota. "Highly Efficient Development of Powertrain Systems Using 1D Real-Time Engine Model." SAE Technical Papers on CD-ROM/SAE Technical Paper Series, September 29, 2023. https://doi.org/10.4271/2023-32-0154
[19] Forte, Ansys. "Forte Theory Manual 18.2." (2020). https://www.scribd.com/document/536366549/ANSYS-Forte-Theory-Manual-18-2